JOURNAL OF MATERIALS SCIENCE **40** (2005) 6291–6299

Geometrical analysis and pattern recognition using mapping technologies of three-dimensional fracture surfaces in materials

M. TANAKA*
Research Institute of Materials and Resources, Department of Mechanical Engineering,Akita University, 1-1 Tegatagakuen-cho, Akita 010-8502, Japan
E-mail: tanaka@mech.akita-u.ac.jp

Y. KIMURA
Nippon System Ware Company

A. KAYAMA
Furukawa Company

J. TAGUCHI
Graduate School, Akita University

R. KATO
Research Institute of Materials and Resources, Department of Mechanical Engineering,Akita University, 1-1 Tegatagakuen-cho, Akita 010-8502, Japan

Published online: 8 September 2005

Geometrical analysis of fracture surfaces in materials was made using newly developed computer programs on the three-dimensional images reconstructed by the stereo matching method. The global value of the fractal dimension of the fracture surface was estimated by the box-counting method on a fatigue fracture surface of a Cu-Be alloy and impact fracture surfaces of a SiC and an alumina. The results of the present analysis were well correlated with those of the two-dimensional fractal analysis. The fractal dimension map (FDM) by the box-counting method and the surface roughness map (SRM) proposed in this study can give important information about the local fracture mechanisms, the crack growth direction or the fracture origin in materials. FDM and SRM have interesting characteristics by which one can discriminate the flat regions, the regions of complex geometry or the steeply inclined areas on a given fracture surface. Pattern recognition using mapping technologies of FDM and SRM is also applicable to the extraction of "hidden patterns" on fracture surfaces, which cannot be observed only by microscopes.

1. Introduction

Mandelbrot *et al*. [1] first characterised the fracture surfaces of impact-loaded and fractured steels by the two-dimensional fractal dimension (D', $1 < D' < 2$). The fractal dimension of the fracture surfaces is generally affected by microstructures or fracture mechanisms of materials [2–5]. The fractal dimension of the fracture surface profile (D'', $1 < D'' < 2$) is larger in the ductile fracture surfaces than in the brittle fracture surfaces such as grain-boundary facets in the creep-ruptured specimens [3] or in the fatigue fractured specimens [4] of metallic materials. These fractal dimensions are the global values, which represent the principal feature of fracture surfaces. Gokhale *et al*. [6] have reported that there is a local variation in the fracture surface patterns of materials. Difference in the fracture mechanisms may lead to a variety of micro fracture patterns [2, 3, 7–9]. The fractal dimension of the fracture surface profile (D″) decreases with crack growth and with increasing creep stress in the austenitic 21Cr·4Ni·9Mn heat-resisting steels [10].

Characteristic patterns on fracture surfaces of materials can be observed using a scanning electron microscope (SEM) or a scanning probe microscope (SPM) such as a scanning electron microscope (STM) and an atomic force microscope (AFM) [8, 11, 12]. However, SPMs are not suitable for the observation of complex fracture surfaces, which involve ledges and dimples.

*Author to whom all correspondence should be addressed.
0022-2461
DOI: 10.1007/s10853-005-3140-z

Computer-aided stereo matching method has been successfully applied to the reconstruction and analysis of three-dimensional images of fracture surfaces in materials [13–16]. Kimura *et al*. [17] have recently developed a new stereo matching method on the basis of the coarse-to-fine formula, which has enabled fast three-dimensional image reconstruction with reasonable accuracy. The authors applied this method to the estimation of the fractal dimensions of the contours and the fracture surface profiles on the fatigue-fractured specimen of a Cu·Be alloy [18].

It is important to estimate directly the global value of the fractal dimension on fracture surfaces (D, $2 < D < 3$) in three-dimensional space, while the three-dimensional fractal dimension (D) can be predicted from the two-dimensional value when a given fracture surface is "isotropic" [19]. Several methods have been proposed for evaluation of the three-dimensional fractal dimension [11, 19–22]. According to the previous study of the two-dimensional analysis [9, 10, 23, 24], the present authors developed a computer program of the box-counting method for the estimation of the fractal dimension of the three-dimensional fracture surfaces [25]. The global value of the fractal dimension was estimated on the three-dimensional fracture surfaces of metals and ceramics reconstructed by the stereo matching method in this study. The results of the present fractal analysis were then compared with those of the two-dimensional fractal analysis [4, 18, 26].

The surface roughness as well as the fractal dimension may give useful information of local fracture patterns on fracture surfaces. Analysis of local fracture patterns on a given fracture surface can be made by mapping the values of the fractal dimension and the surface roughness as two-dimensional images (maps) and by examining these two maps. In this study, computer programs of the fractal dimension map (FDM) by the box-counting method and of the surface roughness map (SRM) were developed for the investigation of local variations in the fracture surface patterns and the fracture mechanisms of materials. Mapping technologies were then applied to the analysis of the reconstructed three·dimensional fracture surfaces of a Cu-Be alloy, a silicon carbide (SiC) and a commercial alumina. Characteristics of FDM and SRM were also discussed on the basis of the analytical results.

2. Analysed fracture surfaces of materials

Materials used for analysis of fracture surface geometry are a Cu-Be alloy (C17200, Cu-1.9 wt% Be-0.3 wt% Co) [4], a silicon carbide (SiC) (Norton NC-430) [26–28] and a commercial alumina (SSA-H, 95.3 wt% Al_2O_3-2.8 wt% SiO_2-1.5 wt% MgO). SSA-H alumina is often used for heat insulator of thermocouples. A fatigue fracture surface was produced by repeated bending on the rectangular specimen (1.5 mm thickness, 10 mm width and 144 mm length) of a Cu-Be alloy (the maximum total strain range is 0.0171) [4]. Impact fracture surfaces were produced by impact loading at a corner of a rectangular sample (6 × 13 × 25 mm) of a SiC (Norton NC-430) and on a side of a tubular sample (2.5 mm outer diameter, 1.5 mm inner diameter and 100 mm length) of an alumina (SSA-H).

Photographs of stereo pairs (basic image and another image tilted by 10 deg) on fracture surfaces were taken using a scanning electron microscope (SEM). The photographs were then taken into a computer and were converted to the digital images of 256 grey scale levels. Three-dimensional image reconstruction was carried out using these stereo pair images by the computer program of the stereo matching method developed by Kimura *et al*. [17]. The height data of a fracture surface for geometrical analysis were extracted from the reconstructed three-dimensional image, and were displayed as a height image. Therefore, the height on the fracture surface increases with increasing colour number (brightness) from 0 to 255, and the brightest region corresponds to the highest part on the fracture surface.

3. Analytical methods

A computer program of the box-counting method was developed for the estimation of the fractal dimension of the three-dimensional fracture surface in the previous study [25]. The fractal analysis was made using the height images (256 grey scale levels) extracted from the reconstructed three-dimensional images in this study, although the numerical height data were also available in this program. Therefore, the height data (z-direction) were given by the colour number (from 0 to 255), and the distance data were given in pixel in the two perpendicular directions (in the x-y plane). In the computer program, three-dimensional fracture surfaces are covered with boxes of rectangular parallelepiped shape with the side length r in the x- and y-directions and with the height cr in the z-direction where c is a constant (Fig. 1). The scale for the fractal analysis is considered to be $(cr^3)^{1/3}$ in this case. The number of boxes (N) covering the fracture surface can be related to the "box size" (r) through the three-dimensional fractal dimension (D) by the following power law relationship:

$$N \propto \left\{(cr^3)^{1/3}\right\}^{-D} \propto r^{-D} \tag{1}$$

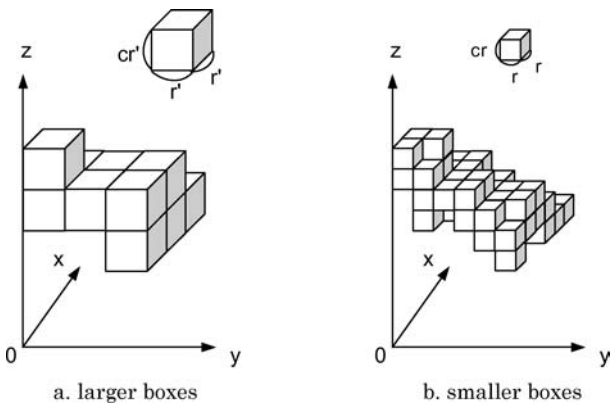

Figure 1 Schematic illustration of the box-counting method for the fractal analysis using boxes of rectangular parallelepiped shape, which cover a three-dimensional fracture surface (r and r' are the side length and c is a constant).

where $c^{-D/3}$ is a constant. Equation 1 can also be written as

$$\log N \propto -D \log r \tag{2}$$

The fractal dimension, D, can be calculated from Equation 2 by the regression analysis using the datum sets of N and r. The fractal dimension was estimated in the scale length (r) range from 2 pixels to a given size in this study.

The surface roughness, rms, in a given area of $m \times m$ pixels was calculated by the following equation [11]:

$$\text{rms} = \sqrt{\sum_{x=1}^{m}\sum_{y=1}^{m}\frac{\{z(x,y)-Z\}^2}{m^2-1}} \tag{3}$$

where $z(x, y)$ is the height of a point $P(x, y)$ and $Z = \sum_{i=1}^{m}\sum_{j=1}^{m}\frac{z(i,j)}{m^2}$.

Computer programs of the fractal dimension map (FDM) by the box-counting method and the surface roughness map (SRM) were also developed to investigate the micro fracture patterns on fracture surfaces. Fig. 2 shows the procedure of the calculation and mapping of shape parameters in an image. The local values of the fractal dimension or those of the surface roughness were calculated by Equation 2 or 3 using the height data. The calculated area was moved in both x- and y-directions by k pixels in mapping process. The results of the calculation were finally displayed in colour number in the central part of $k \times k$ pixels, and therefore, the brightest area in FDM or SRM corresponds to the part of the largest value of the fractal dimension or the surface roughness. The length scale (r) for mapping the fractal dimension was in the range from 2 pixels to the size of calculated area (m pixels). Computer programs were made using Visual Basic 6.0.

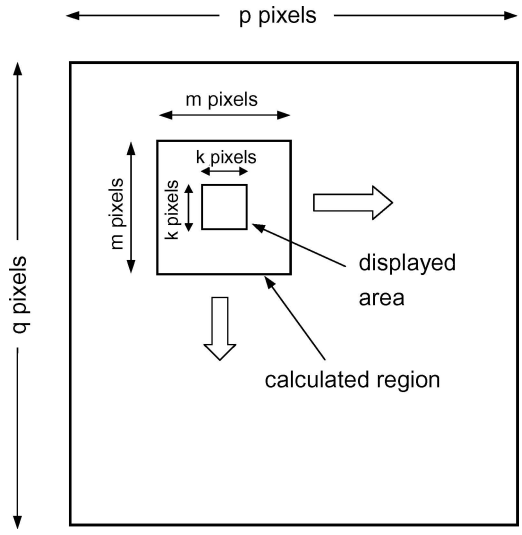

Figure 2 Schematic illustration of the displayed area ($k \times k$ in pixel) centered at the calculated region ($m \times m$ in pixel) in an image ($p \times q$ in pixel) in the calculation and mapping of shape parameters.

4. Results and discussion

4.1. Global fractal dimension of fracture surfaces

Fig. 3 shows the original SEM image and the height image produced by the three-dimensional image reconstruction of fracture surfaces in materials. The computed area for three-dimensional image reconstruction is enclosed by a square in the original SEM images (Figs 3a–c). In the original images, one pixel corresponds to about 1.81×10^{-7} m in a Cu-Be alloy (C17200), about 1.49×10^{-7} m in an alumina (SSA-H) and about 1.13×10^{-7} m in a SiC (Norton NC-430). Ductile fracture surfaces which are composed of small slip steps and dimples, are principally observed on the stage I fatigue fracture surface of a Cu-Be alloy (C17200), although grain-boundary facets are also visible (Fig. 3a) [4]. Mixed mode fracture in this alloy will be analysed in the next section. The crack growth direction is approximately from right to left in Fig. 3a. Central part of the original image seems to be the highest, as known from the height image (Fig. 3d). Relatively flat region can be seen in the central part of the impact fracture surface in a SiC (Norton NC-430), while other regions seem to be a little rougher (Fig. 3b). The height image shows that the flat region is higher than other regions (Fig. 3e). The flat region may be created by fracture at the interface between a large SiC particle and residual silicon (Si), whereas the rougher regions are probably formed by fracture at the interface between the smaller SiC particles and residual Si, and also by fracture in the residual Si [25–27]. Characteristic fracture patterns cannot be observed on the impact fracture surface (Fig. 3c) and the height image (Fig. 3f) of an alumina (SSA-H), except microvoids, which are probably formed during sintering (Fig. 3c). The fracture surface may be created by fracture in alumina grains and at the grain boundaries, although it is not clear on the image of low magnification.

Fig. 4 shows the bird's eye-view of the stage I fatigue fracture surface in a Cu-Be alloy. The direction of fatigue crack growth is from lower right to upper left in the figure. As known from the figure, there are considerable ups and downs on the fracture surface. Relatively flat region can be observed near the top of the fracture surface. The impact fracture surface of a SiC has also a complex geometry (Fig. 5), although the height difference between the highest part and the lowest part is smaller than that of a Cu-Be alloy (Fig. 4). Fig. 6 shows the bird's eye-view of the impact fracture surface in an alumina. The fracture surface goes up from lower right to upper left, but is relatively flat except very small ledges and bumps.

Fig. 7 shows the global value of the fractal dimension of the fracture surface in materials. The fractal dimension of the fracture surface in a Cu-Be alloy was estimated on a given area of 360 pixels $\times$ 360 pixels (about 6.5×10^{-5} m $\times$ 6.5×10^{-5} m) in the length scale (r) range smaller than one grain-boundary length (from 2 pixels (about 3.6×10^{-7} m) to 72 pixels (about 1.3×10^{-5} m)). The value of the fractal dimension is about 2.16, and is close to the values, 2.190 or 2.210, predicted from the fractal dimension of the ac-

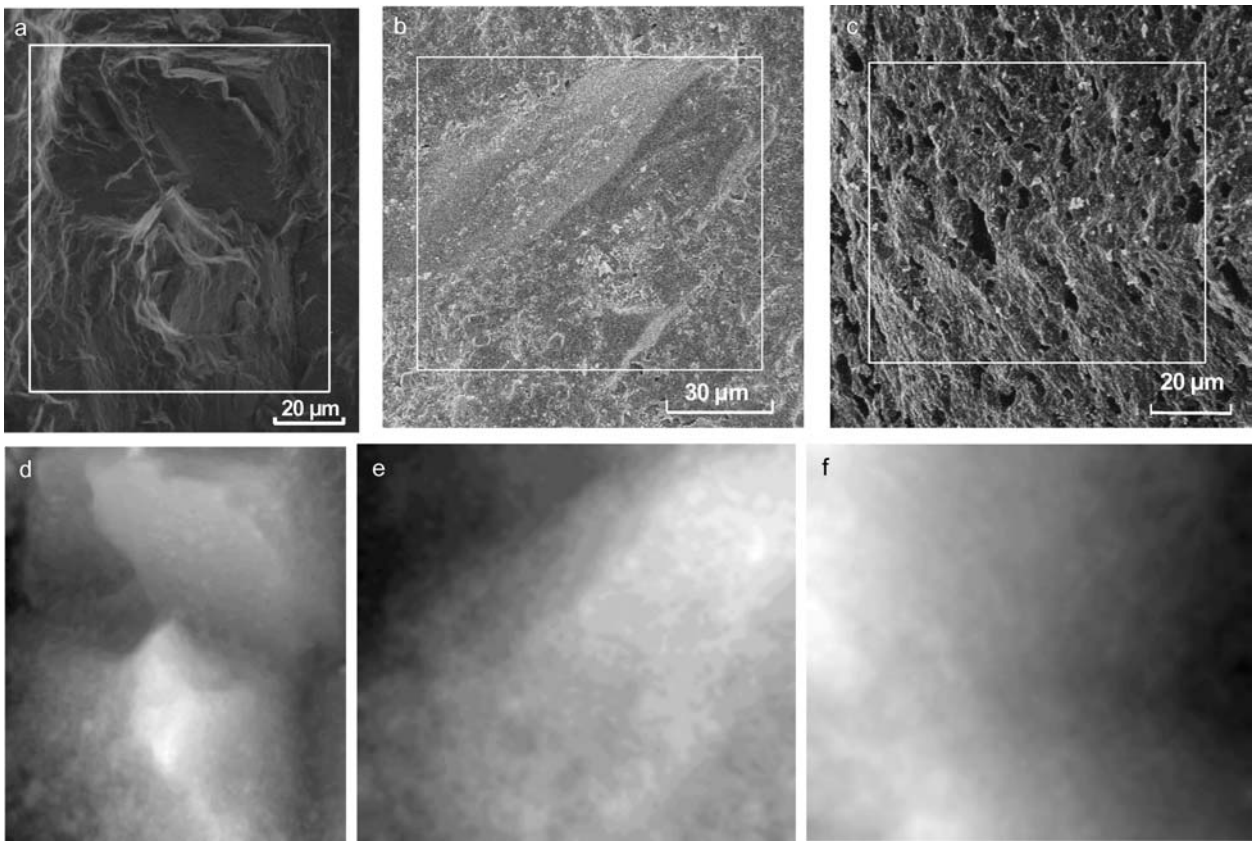

Figure 3 Original SEM images and height images produced by the three-dimensional image reconstruction of the fracture surfaces in materials. a, d: Stage I fatigue fracture surface of a Cu-Be alloy (C17200) (computed area is 403 × 467 pixels) b, e: impact fracture surface of a SiC (Norton NC-430) (computed area is 663 × 601 pixels) c, f: impact fracture surface of an alumina (SSA-H) (computed area is 575 × 513 pixels) (a, b, c: original SEM images and computed area for three-dimensional image reconstruction is enclosed by white lines, d, e, f: height images).

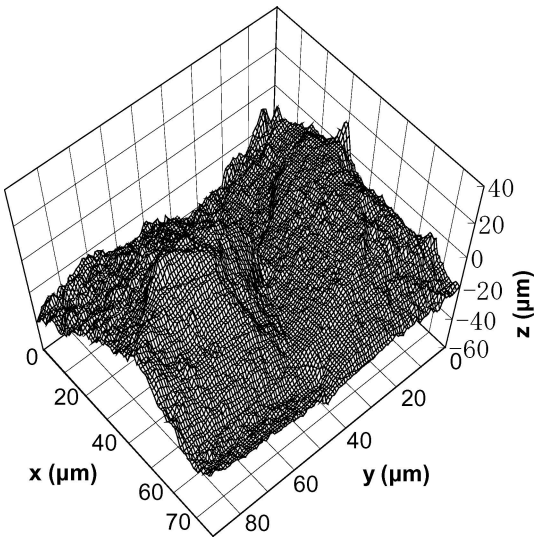

Figure 4 Bird's eye-view of the stage I fatigue fracture surface in a Cu-Be alloy.

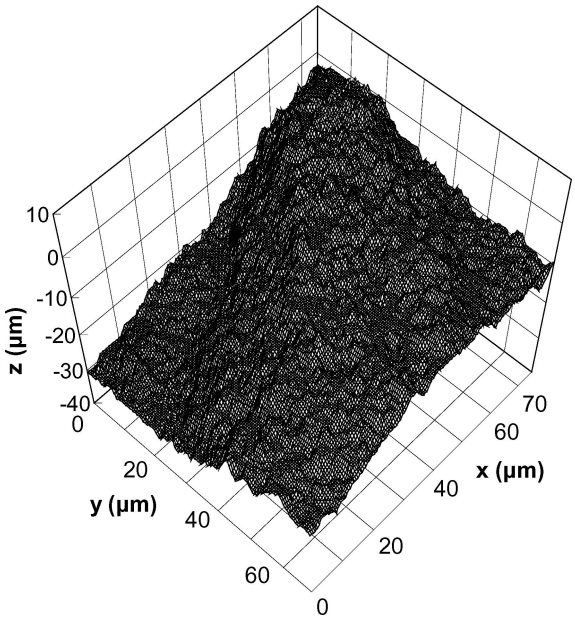

Figure 5 Bird's eye-view of the impact fracture surface in a SiC.

tual fracture surface profile (1.190 or 1.210) estimated in the similar length scale range (from 6.7×10^{-7} to 1.7×10^{-5} m) [4, 18]. Further, the fractal dimension, about 2.16, is almost the same as the values, 2.13 or 2.15, predicted from the fractal dimension of the reconstructed fracture surface profile (1.13 or 1.15) [18]. The analysed area was 600 × 600 pixels (about 6.8×10^{-5} m × 6.8×10^{-5} m) in the impact-fractured specimen of a SiC. The fractal dimension of the three-dimensional fracture surface was about 2.19 in the length scale (r) range from 2 pixels (about 2.3×10^{-7} m) to 50 pixels (about 5.7×10^{-6} m), and could be correlated with the upper bound value, about 2.16, predicted from the fractal dimension of the indentation crack (about 1.16) in the same material. The analysed area was 480 × 480 pixels (about 7.1×10^{-5} m × 7.1×10^{-5} m) in an impact-fractured specimen of an alumina. The three-dimensional fractal dimension is about 2.13, which is

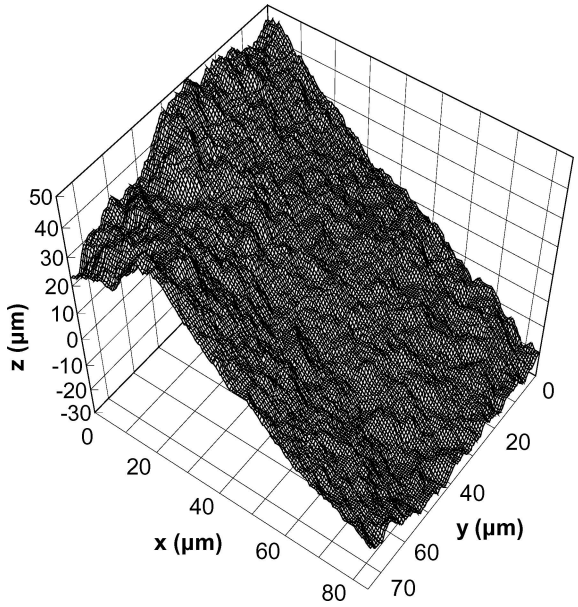

Figure 6 Bird's eye-view of the impact fracture surface in an alumina.

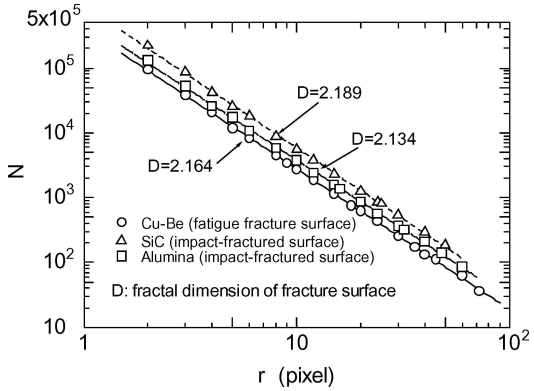

Figure 7 Global value of the fractal dimension of the fracture surface in materials (N: the number of the boxes covering the fracture surface, r: the side length (box size)).

close to the value, about 2.15 to 2.19, predicted from the fractal dimension of the indentation crack (about 1.15 to 1.19) estimated on similar aluminas by the box-counting method [26]. The length scale of the three-dimensional fractal analysis was in the range 2 pixels (about 3.0×10^{-7} m) to 60 pixels (about 8.9×10^{-6} m), and all length scale ranges of the two-dimensional fractal analysis lay between 2.7×10^{-8} m and 1.1×10^{-5} m, although the scale length range was different with each alumina [26].

4.2. Local variation of fracture surface patterns

4.2.1. Fatigue fracture surface of a Cu-Be alloy

The fractal dimension estimated in Section 4.1 is considered as an averaged value of characteristic patterns on a given fracture surface. The fractal dimension map (FDM) and the surface roughness map (SRM) are proposed in order to know the local fracture mechanisms, the crack growth direction or the fracture origin in materials. Fig. 8 shows the original SEM image, FDM and SRM on the stage I fatigue fracture surface of a Cu-Be alloy. The calculated area is 24 × 24 pixels and the displayed area is 4 × 4 pixels in FDM (Fig. 8b) and SRM (Fig. 8c). The value ranges of the fractal dimension and the surface roughness are also shown in the figure. The brighter part shows the region with the larger fractal dimension in FDM or that with the larger surface roughness in SRM. As described in the previous section (Section 4.1), the fatigue fracture surface was formed for the most part in a ductile manner (Fig. 8a). The part of ductile fracture is indicated by the bright region in FDM, while this part does not always show a bright contrast in SRM. The flat part with the fractal dimension of around 2.17 (dark regions in both FDM and SRM) may be formed by grain-boundary fracture, since the fractal dimension of the fatigue fracture surface profile is 1.168 on the stage II fatigue fracture surface of the same alloy where grain-boundary fractures prevails [4]. This part is also shown by broken lines in the maps composed under different conditions of sizes of calculated area (m) and displayed area (k) (Fig. 9). Principal features of FDM and SRM do not significantly change with conditions of calculation and display. The decrease of the displayed area enabled a precise detection of local fracture patterns using FDM and SRM (compare Figs 9a and d with Figs 9b and e), although some patterns become unclear with decreasing displayed area (k). The increase of the calculated area (m) reduced noises in the maps, especially in FDM. However, both increases of the size of calculated area (m) and that of displayed area (k) result in broad fracture patterns (Figs 9c and f). The increase of the calculated area (m) led to the increase of the value range of the surface roughness and to a slight decrease of the value range of the fractal dimension. The steeply inclined part also shows a dark contrast in FDM, but this part is very bright in SRM, irrespective of local fracture mechanisms. Characteristics of FDM and SRM will be discussed later.

4.2.2. Impact fracture surface of ceramics

Fig. 10 shows the original SEM image, FDM and SRM on the impact fracture surface of a SiC. A local variation of fracture patterns can be observed in both maps (Figs 10c and d). Areas of bright contrast in FDM (large fractal dimension) and intermediate contrast in SRM correspond to regions of complex geometry. There are "river-like" patterns, which are dark in FDM (Fig. 10c) and show a bright contrast in SRM (Fig. 10d), and these are considered as steeply inclined parts. As shown in the schematic illustration (Fig. 10b), these "rivers" seem to join at some places and the local crack growth direction can be identified from these patterns (indicated by an arrow in Fig. 10b). Further, there are relatively flat areas, which show a dark contrast in both FDM (Fig. 10c) and SRM (Fig. 10d). Some of them are illustrated in Fig. 10b, and are considered as the regions where brittle-type fracture occurred. These characteristic patterns cannot be detected in the original SEM image (Fig. 10a). As marked by broken lines in Fig. 11, these features seem to be retained even when mapping conditions, namely, the size of calculated area (m) and

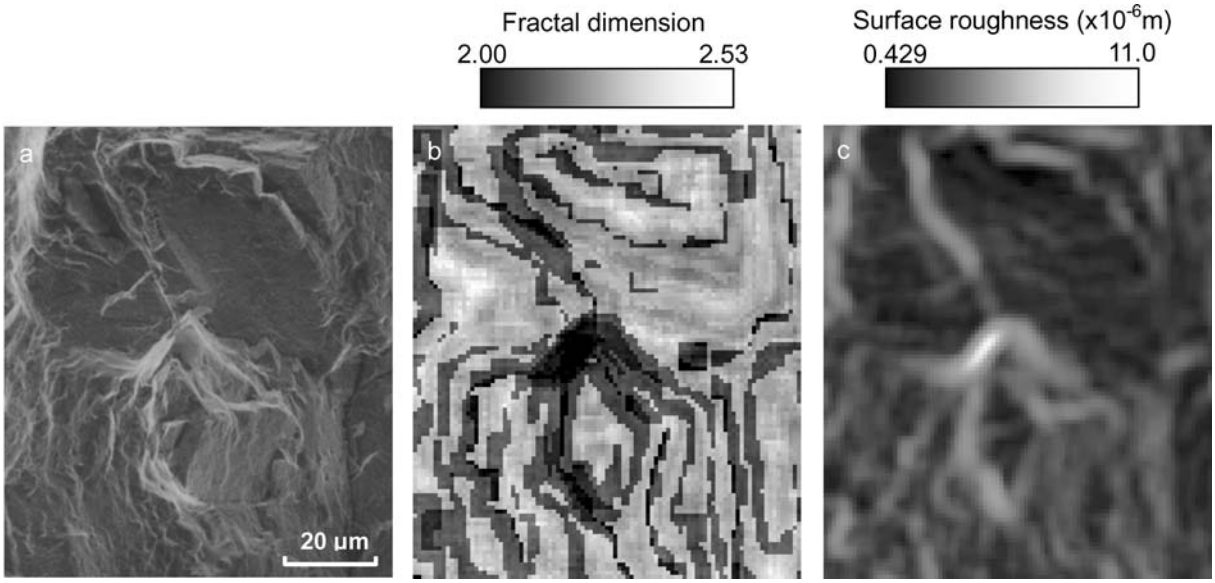

Figure 8 Stage I fatigue fracture surface of a Cu-Be alloy. (a) Original SEM image (403 × 467 pixels) (b) FDM (c) SRM (the calculated area is 24 × 24 pixels and the displayed area is 4 × 4 pixels in b and c).

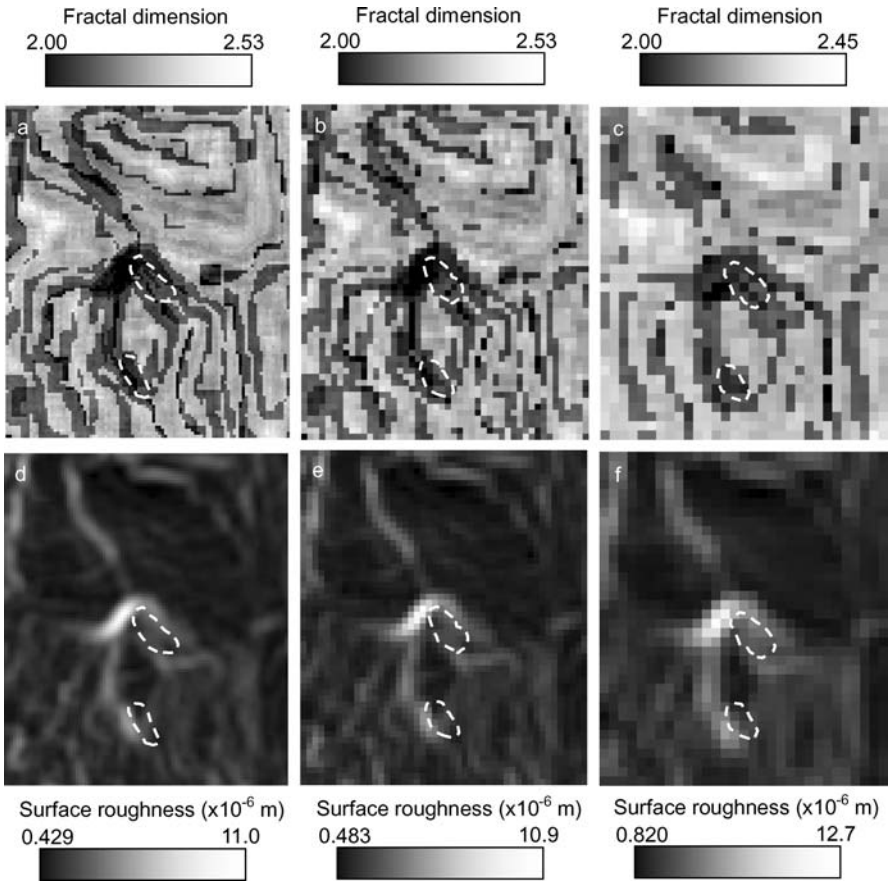

Figure 9 FDM and SRM on the stage I fatigue fracture surface of a Cu-Be alloy. (a) FDM ($m = 24$, $k = 4$) (b) FDM ($m = 24$, $k = 8$) (c) FDM ($m = 36$, $k = 12$) (c) SRM ($m = 24$, $k = 4$) (b) SRM ($m = 24$, $k = 8$) (c) SRM ($m = 36$, $k = 12$) (m is the size of calculated area in pixel and k is the size of displayed area in pixel. The areas enclosed by broken line are identified as the regions where grain-boundary fracture occurred).

displayed area (k) are changed in both FDM and SRM, although changes in mapping conditions may lead to the extinction and emergence of some local patterns. Therefore, it is necessary to choose proper mapping conditions of FDM and SRM for extraction of characteristic patterns on the fracture surfaces of materials.

Similar "river-like" patterns and their joining are observed on the impact fracture surface of an alumina (Fig. 12). By comparing FDM with SRM, one can discriminate the areas of complex geometry, the flat areas and the steeply inclined parts. The "River-like" patterns are much clearer in FDM (Fig. 12c) than in SRM (Fig. 12d) in this case. Joining of "rivers" is visible at some places and the local crack growth direction (approximately from top to bottom) can be identified as schematically illustrated in Fig. 12b, although the

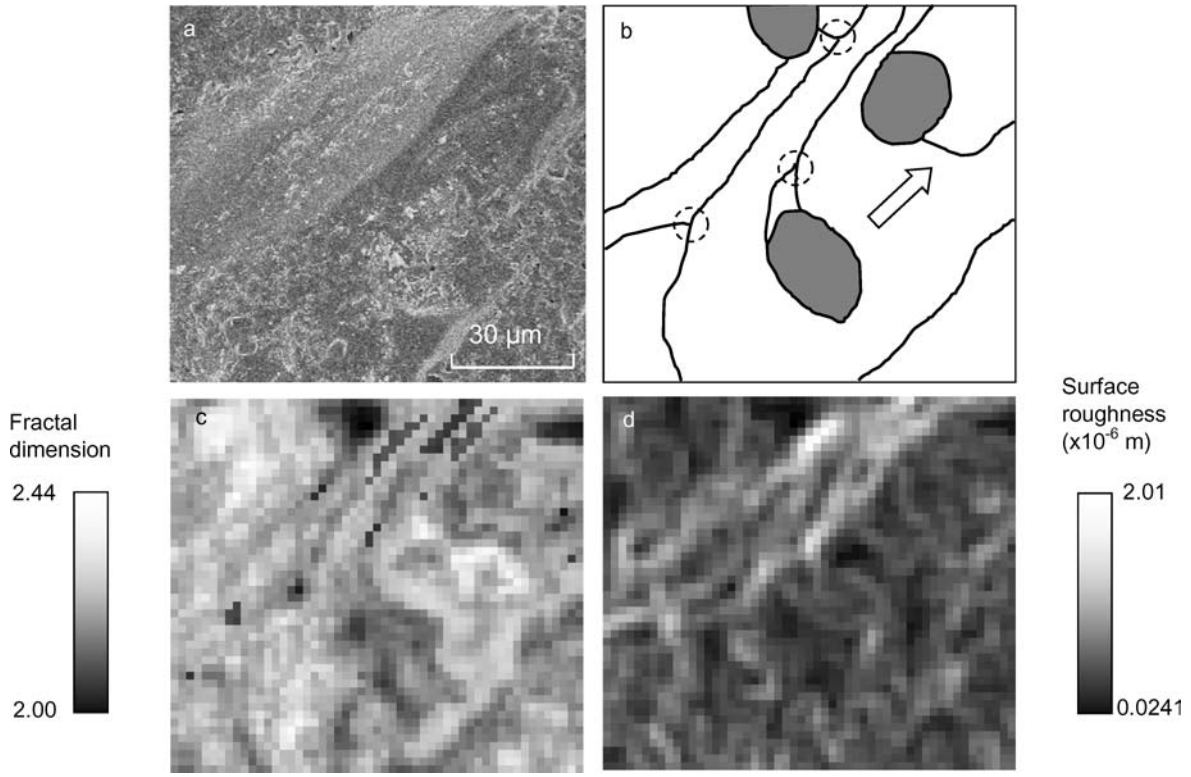

Figure 10 Impact fracture surface of a SiC. (a) Original SEM image (663 × 601 pixels) (b) schematic illustration (lines show river-like patterns, marked areas are considered as the regions where "brittle fracture" occurred, and an arrow indicates the local crack growth direction known by the joining of "rivers" (shown by broken circles) (c) FDM (d) SRM (the calculated area is 36 × 36 pixels and the displayed area is 12 × 12 pixels in c and d).

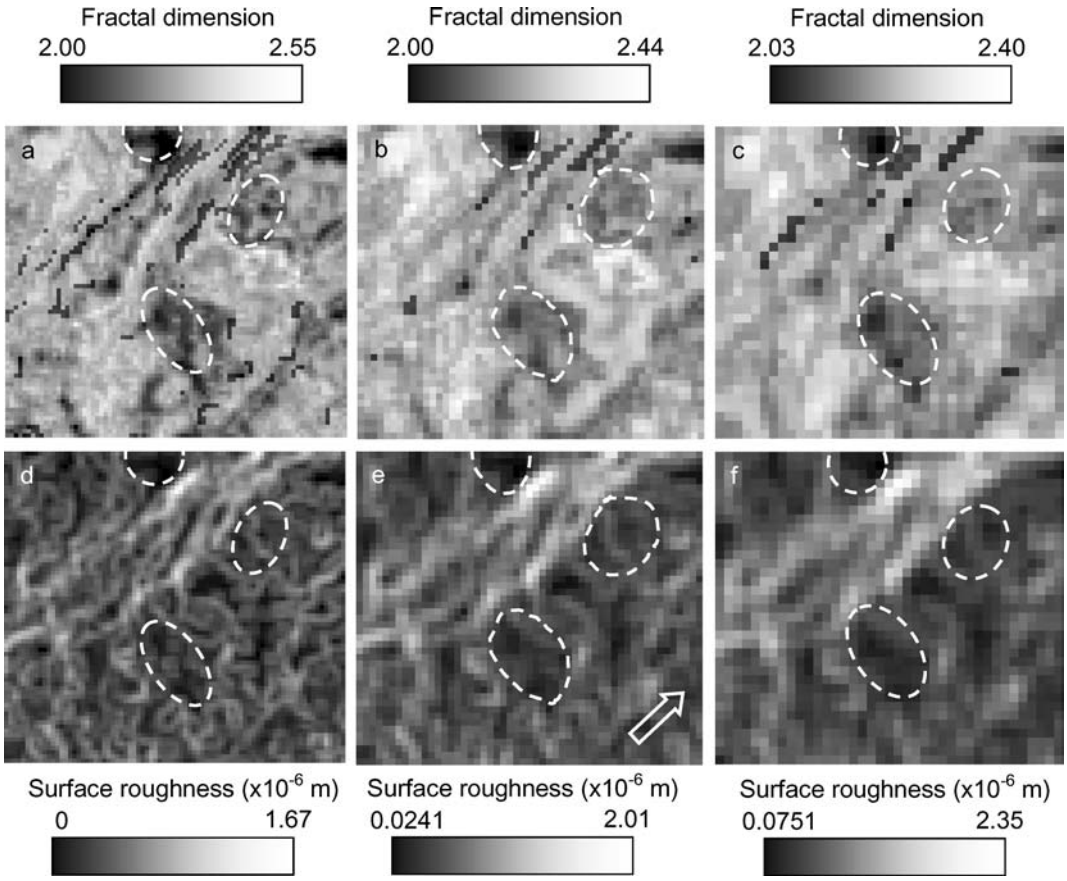

Figure 11 FDM and SRM on the impact fracture surface of a SiC. (a) FDM ($m = 24$, $k = 8$) (b) FDM ($m = 36$, $k = 12$) (c) FDM ($m = 48$, $k = 16$) (c) SRM ($m = 24$, $k = 8$) (b) SRM ($m = 36$, $k = 12$) (c) SRM ($m = 48$, $k = 16$) (m is the size of calculated area in pixel and k is the size of displayed area in pixel. An arrow shows the local crack growth direction and broken circles show the regions of brittle fracture.).

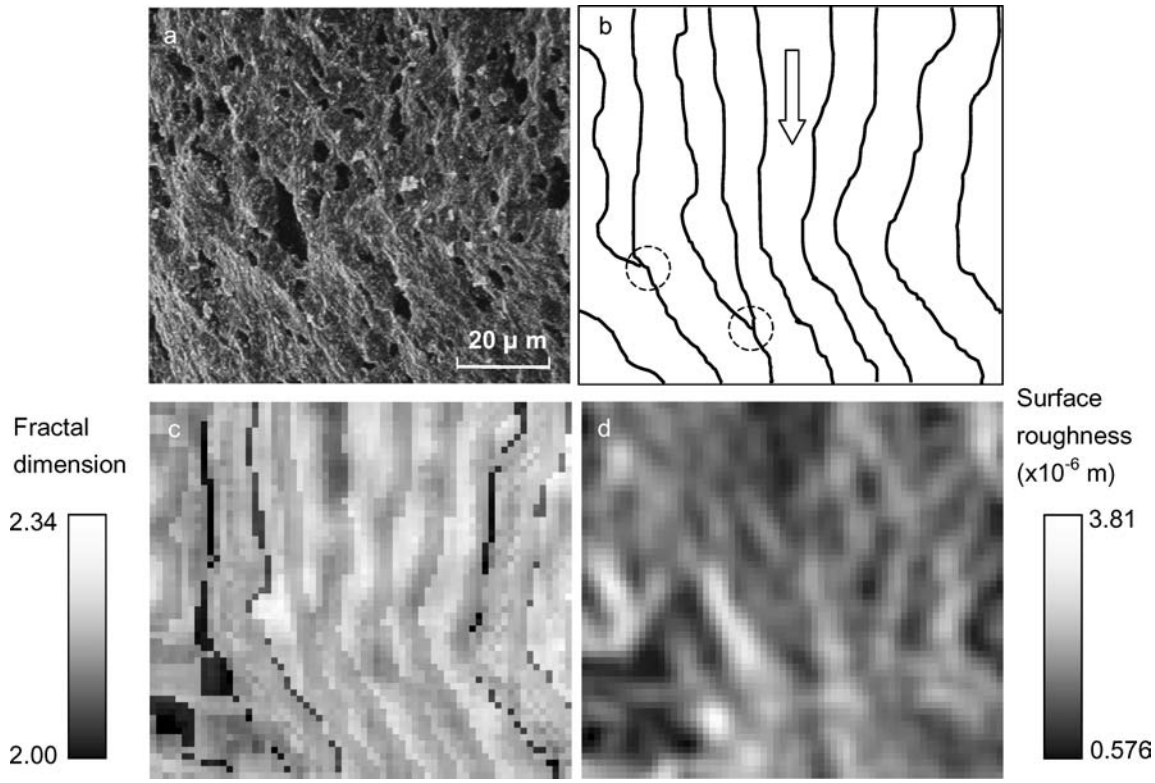

Figure 12 Impact-fractured surface of an alumina. (a) Original SEM image (575 × 513 pixels) (b) schematic illustration (lines indicate "river-like" patterns and an arrow shows the main crack growth direction known from the joining of "rivers" (shown by broken circles) (c) FDM d. SRM (the calculated area is 48 × 48 pixels and the displayed area is 8 × 8 pixels in c and d).

fracture origin does not seem to exist in the original SEM image (Fig. 12a). Characteristic patterns such as the "river-like" patterns are not visible in the original micrograph (Fig. 12a). It is worth noting that FDM and SRM can detect the patterns that cannot be observed by microscopy. Thus, one may gain information on the local fracture mechanisms, the crack growth direction or the fracture origin in a given fracture surface using FDM and SRM.

4.3. Characteristics of FDM and SRM

The following characteristics can be deduced from the on FDM and SRM analytical results on the fracture surfaces of materials in Section 4.2:

(1) An area of bright contrast in FDM but not always bright contrast in SRM corresponds to a region of relatively complex geometry (bright in FDM and bright or intermediate in SRM).
(2) A part of dark contrast in both FDM and SRM corresponds to a relatively flat region such as a brittle fracture surface (dark in both FDM and SRM).
(3) A part of dark contrast in FDM and bright contrast in SRM corresponds to a steeply inclined part. This part apparently shows the smaller fractal dimension and the larger surface roughness, irrespective of fracture mechanisms (dark in FDM and bright in SRM).

Therefore, local fracture patterns can be determined from inspection of these characteristics on a given fracture surface. A schematic illustration shows how a fracture surface can be observed by tilting (Fig. 13). By considering the direction of observation on the fracture

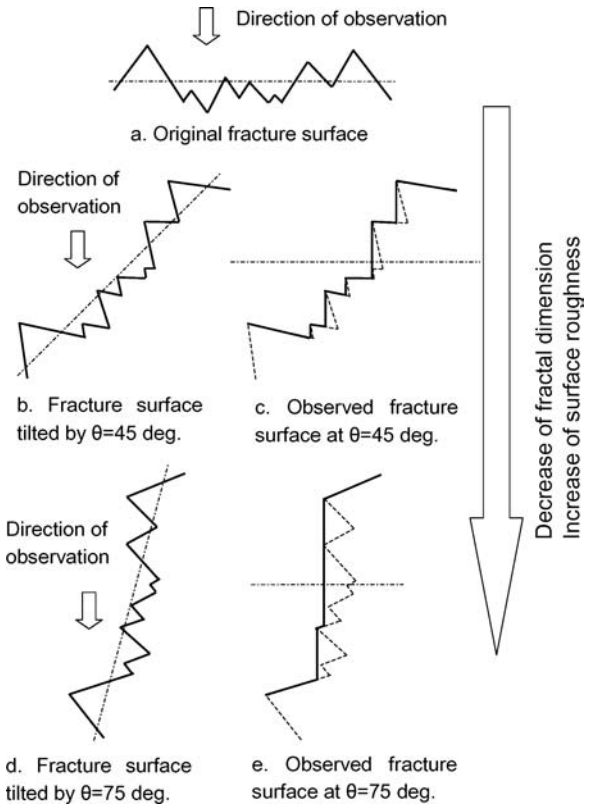

Figure 13 Schematic illustration showing how a fracture surface can be observed by tilting.

surface, it is clear that ledges and bumps (Fig. 13a) are only partly detectable on the steeply inclined fracture surface and the observed fracture surface becomes simpler (Fig. 13e). The difference between the max-

imum height and the minimum height increases with inclination of the fracture surface (Figs 13c and e), and this leads to a larger value of the surface roughness. Thus, a steeply inclined part shows a smaller value of the fractal dimension and a larger value of the surface roughness, irrespective of the original surface geometry. This part is shown as a dark region in FDM and as a bright region in SRM. In a fracture surface containing steeply inclined parts, some patterns may not be observed in FDM or SRM but other characteristic patterns, which cannot be observed in the original image, may become clear in FDM or SRM. These patterns in FDM or SRM give a clue for investigation of the local fracture mechanisms, the crack growth direction or the fracture origin in a given fracture surface. Pattern extraction using mapping technologies of FDM and SRM enables "hidden patterns" on fracture surfaces to be interpreted in terms of fractography.

5. Conclusions

(1) Three-dimensional fracture surfaces of materials reconstructed by the stereo matching method were analysed using newly developed computer programs. The global value of the fractal dimension was estimated on the stage I fatigue fracture surface of a Cu-Be alloy and the impact fracture surfaces of a silicon carbide (SiC) and a commercial alumina. The results of the present analysis were well correlated with those predicted by the two-dimensional fractal analysis.

(2) Rough surface regions, flat regions and steeply inclined parts respectively showed different contrast in the fractal dimension map (FDM) and the surface roughness map (SRM) of fracture surfaces developed in this study. FDM and SRM could detect the regions of ductile fracture, those of grain-boundary fracture and the steeply inclined areas in the fatigue fracture surface of a Cu-Be alloy. "River-like" patterns or the regions of brittle-type fracture, which was not observed in the scanning electron microscope (SEM) image, was recognized using FDM and SRM on the impact fracture surfaces of a SiC and an alumina.

(3) It is necessary to choose proper mapping conditions for FDM and SRM for extracting characteristic fracture patterns. Pattern recognition using mapping technologies of FDM and SRM is applicable not only to the investigation of the local fracture mechanisms, the crack growth direction or the fracture origin but also to the extraction of "hidden patterns" on fracture surfaces of materials.

Acknowledgments

The authors thank The Iron and Steel Institute of Japan (Grant-in-Aid [b]) and Mitsutoyo Association for Science and Technology (MAST) for financial support.

References

1. B. B. MANDELBROT, D. E. PASSOJA and A. J. PAULLAY, *Nature* **308** (1984) 721.
2. R. H. DAUSKARDT, F. HAUBENSAK and R. O. RITCHIE, *Acta Metall.* **38** (1990) 142.
3. M. TANAKA, *J. Mater. Sci.* **27** (1992) 4717.
4. M. TANAKA, A. KAYAMA and R. KATO, *J. Mater. Sci. Lett.* **18** (1999) 107.
5. X. W. LI, J. F. TIAN, S. X. LI and Z. G. WANG, *Mater. Trans.* **42** (2001) 128.
6. A. M. GOKHALE, W. J. DRURY and F. MISHRA, ASTM STP1203, edited by J. E. Masters and L. N. Gilbertson (American Society for Testing and Materials, Philadelphia, PA, 1993) p. 3.
7. Z. G. WANG, D. L. CHEN, X. X. JIANG, S. H. AI and C. H. SHIH, *Scripta Metall.* **22** (1988) 827.
8. S. MATSUOKA, H. SUMIYOSHI and K. ISHIKAWA, *Trans. Japan Soc. Mech. Eng.* **56** (1990) 2091.
9. M. TANAKA, A. KAYAMA, R. KATO and Y. ITO, *Fractals* **3** (1999) 335.
10. M. TANAKA, *Z. Metallkd.* **88** (1997) 217.
11. N. ALMQVIST, *Surf. Sci.* **355** (1996) 221.
12. V. Y. MILMAN, N. A. STELMASHENKO and R. BLUMENFELD, *Progr Mater. Sci.* **38** (1994) 425.
13. K. KOMAI and J. KIKUCHI, *J. Soc. Mater. Sci. Japan* **34** (1985) 648.
14. T. KOBAYASHI and D. A. SHOCKEY, *Metall. Trans.* **18A** (1987) 1941.
15. J. STAMPFL, S. SCHERER, M. BERCHTHALER, M. GRUBER and O. KOLEDNIK, *Int. J. Fract.* **78** (1996) 35.
16. J. STAMPFL and O. KOLEDNIK, *ibid.* **101** (2000) 321.
17. Y. KIMURA, M. TANAKA and R. KATO, *ISIJ International (Note)* **44** (2004), 1276. Y. KIMURA and M. TANAKA, Proceedings of the Fourth International Conference on Materials for Resources, Akita, Japan, October 11–13, 2001, vol. 2, pp. 249.
18. M. TANAKA, Y. KIMURA, L. CHOUANINE, J. TAGUCHI and R. KATO, *ISIJ International* **43** (2003), 1453.
19. H. TAKAYASU, Fractals in the Physical Sciences. (Manchester University Press, Manchester and New York, 1990), p. 6.
20. B. B. MANDELBROT, "The Fractal Geometry of Nature". translated by H. Hironaka (Nikkei Science, Tokyo, 1985) p. 108.
21. D. SEN, S. MAZUMDER and S. TARAFDAR, *J. Mater. Sci.* **37** (2002) 941.
22. U. WENDT, K. STIEBE-LANGE and M. SMID, *J. Microsc.* **207** (2002) 169.
23. M. TANAKA and A. KAYAMA, *J. Mater. Sci. Lett.* **20** (2001) 907.
24. A. KAYAMA, M. TANAKA and R. KATO, *ibid.* **19** (2000) 565.
25. M. TANAKA, Y. KIMURA, L. CHOUANINE, R. KATO and J. TAGUCHI, *ibid.* **22** (2003), 1279.
26. M. TANAKA, *J. Soc. Mater. Sci. Japan* **47** (1998) 169.
27. *Idem.*, *J. Mater. Sci.* **31** (1996) 749.
28. *Idem.*, *J. Mater. Sci. Lett.* **15** (1996) 1184.

Received 5 June 2003
and accepted 4 April 2005